J|A|C|S ARTICLES

Published on Web 04/17/2009

Resistive Molecular Memories: Influence of Molecular Parameters on the Electrical Bistability

Simone Di Motta,[†] Eugenio Di Donato,[†] Fabrizia Negri,*[,†] Giorgio Orlandi,[†] Daniele Fazzi,[‡] and Chiara Castiglioni[‡]

Dipartimento di Chimica "G. Ciamician", Università di Bologna, Via F. Selmi, 2, 40126 Bologna, Italy, and INSTM, UdR Bologna, Italy, and Dipartimento di Chimica, Materiali e Ingegneria Chimica, Politecnico di Milano, "G. Natta", P.zza Leonardo da Vinci 32, 20133 Milano, Italy, and INSTM, UdR Milano, Italy

Received February 12, 2009; E-mail: fabrizia.negri@unibo.it

Abstract: The electrical bistability behavior of 2,3-dichloro-5,6-dicyano-1,4-benzoquinone (DDQ) along with two additional benzoquinone derivatives (TCQ and TCN) and pentacene (PNT) is investigated by computing intra- and intermolecular charge transfer parameters and by comparing the efficiency of bulk charge transport and charge injection at the electrode/organic interface in the presence of neutral and charged molecular species. The bulk charge transport is modeled assuming a charge hopping regime and by computing hopping rates and mobilities. Molecular dynamics simulations are carried out to estimate the effect of thermal disorder on charge transfer integrals. The efficiency of the interface transport is estimated by comparing the electron affinities of benzoquinone derivatives and the ionization potential of pentacene with the work function of commonly employed electrodes. It is shown that the observed memory effect can be rationalized in terms of an interplay of the two transport mechanisms by showing that the OFF state is dominated by interface limited phenomena and the ON state may be determined also by bulk transport limited phenomena. While the contribution of collective effects cannot be ruled out for the macroscopic memory phenomenon, we show that, at a molecular level, sizable intramolecular reorganization energies are fundamental for the efficiency of the device, provided their magnitude does not hamper the charge transport across the device. It is suggested that control over molecular parameters might be exploited to design more efficient resistive molecular memories.

1. Introduction

Organic electronics has been a field of intense research interest for the last couple of decades. Besides light emitting diodes, photovoltaic devices, and field effect transistors, recently, conjugated organic materials displaying memory effects have received considerable attention. Memory effects can be driven by several physical phenomena.[1,2] Here, we refer to organic-based devices in which the memory effect is induced by an electrical stimulus.[3] In these devices, two stable conducting states (hereafter labeled OFF and ON states) exist at the same applied voltage, and one can switch from one state to the other by applying a suitable voltage. Once the device is in the ON state, for instance, it retains its high conductivity until a specific action (reset) is taken by a reverse voltage that erases the ON state and returns the device in its OFF state.[4,5] The rationalization of the change in conductivity is still under debate: in some cases, there is evidence of extrinsic mechanisms (presence of metal filaments, metal nanoparticles) not due to the properties of the molecular material.[3,6] In others, however, there is strong evidence that the mechanism is intrinsic, driven by the nature of the organic material. In some cases, it has been explained in terms of structural rearrangements (conformational changes),[7] or electronic changes induced by redox reactions,[8,9] or both.[10,11]

Further evidence supporting the intrinsic molecular mechanism has been provided by modifying the organic molecule with electron-withdrawing groups (EWG) of different strength and monitoring associated changes in ON/OFF ratios.[8,12] One such example is Rose Bengale (RB) for which the resistive memory efficiency (ON/OFF ratio) has been shown to increase with the strength of EWGs.[12–14] Other studies using devices built with different layers of the deposited organic material have also

[†] Università di Bologna and INSTM.
[‡] Politecnico di Milano and INSTM.

(1) Wełnic, W.; Wuttig, M. *Mater. Today* **2008**, *11*, 20–27.
(2) Ling, Q.-D.; Liaw, D.-J.; Zhu, C.; Chan, D. S.-H.; Kang, E.-T.; Neoh, K.-G. *Prog. Polym. Sci.* **2008**, *33*, 917–978.
(3) Scott, J. C.; Bozano, L. D. *Adv. Mater.* **2007**, *19*, 1452–1463.
(4) Mukherjee, B.; Pal, A. J. *Org. Electron.* **2006**, *7*, 249–255.
(5) Tondelier, D.; Lmimouni, K.; Vuillaume, D.; Fery, C.; Haas, G. *Appl. Phys. Lett.* **2004**, *85*, 5763–5765.
(6) Bozano, L. D.; Kean, B. W.; Deline, V. R.; Salem, J. R.; Scott, J. C. *Appl. Phys. Lett.* **2004**, *84*, 607–609.
(7) Donhauser, Z. J.; Mantooth, B. A.; Kelly, K. F.; Bumm, L. A.; Monnell, J. D.; Stapleton, J. J.; Price, D. W.; Rawlett, A. M.; Allara, D. L.; Tour, J. M.; Weiss, P. S. *Science* **2001**, *292*, 2303–2307.
(8) Bandhopadhyay, A.; Pal, A. J. *J. Phys. Chem. B* **2003**, *107*, 2531–2536.
(9) Chen, J.; Reed, M. A.; Rawlett, A. M.; Tour, J. M. *Science* **1999**, *286*, 1550–1552.
(10) Bandyopadhyay, A.; Pal, A. J. *Appl. Phys. Lett.* **2004**, *84*, 999–1001.
(11) Solak, A. O.; Ranganathan, S.; Itoh, T.; McCreery, R. L. *Electrochem. Solid State Lett.* **2002**, *5*, E43−E46.
(12) Rath, A. K.; Pal, A. J. *Org. Electron.* **2008**, *9*, 495–500.
(13) Majee, S. K.; Bandyopadhyay, A.; Pal, A. J. *Chem. Phys. Lett.* **2004**, *399*, 284–288.
(14) Rath, A. K.; Sahu, S.; Pal, A. J. *Appl. Phys. Lett.* **2006**, *89*, 142110.

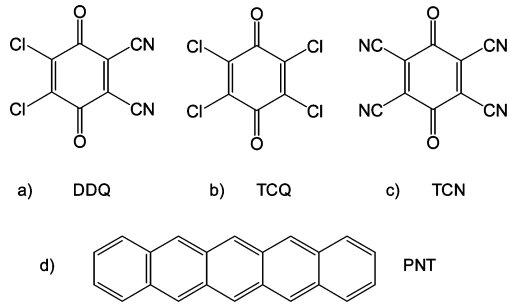

Figure 1. Structural formula of the four molecules considered in this work.

pointed to the intrinsic molecular character of the phenomenon, and at the same time have shown that collective effects are relevant. Indeed, in the case of a single molecular layer, the device was shown to display a threshold switching phenomenon, which becomes a resistive memory behavior[13] only by increasing the number of layers of the organic species and hence sustaining more efficiently the charge density on the device.[13]

Among molecular systems, diphenyl bithiophene (DPBT) derivatives have been shown to display electrical bistability,[15,16] and in a recent computational study[17] it was shown that the different electrical behavior observed for Z and L isomers can be associated with a different efficiency of level alignment at the interface electrode/semiconductor. DPBT derivatives are quite complex molecular systems, with flexible degrees of freedom that can mask or modulate the resulting electric properties. To date, the simplest organic molecule displaying electrical memory behavior[4,8,18−21] is 2,3-dichloro-5,6-dicyano-1,4-benzoquinone (DDQ) (see Figure 1a). Evidence on the molecular nature of the phenomenon has been recently provided by the sensitivity of the ON state current to the work function of the electrodes employed to fabricate the device.[4] Highly conductive organic semiconductors like pentacene have been employed to prepare organic bistable devices,[5] but the memory effect was attributed to the inclusion of metal nanoparticles during electrode evaporation on top of the organic material.[5,22] Indeed, there was no evidence of bistability by gently contacting pentacene on the electrode.[5] These results call for a deeper understanding of the intramolecular and intermolecular parameters governing the intrinsic molecular memory effect, and this is the objective of this study.

Among the processes governing the electrical (or resistive) memory function in molecular materials, the efficiency of carrier injection into the organic material at the electrode/organic interface and the charge transport within the organic semiconductor have to be considered as factors limiting the current. In this Article, we have considered these two processes and have performed a computational investigation to evaluate their relevance for the electrical bistability of DDQ and, to explore the effect of EWGs, two additional benzoquinone (BQ) derivatives, 2,3,5,6-tetrachloro-BQ (TCQ) (see Figure 1b) and 2,3,5,6-tetracyano-BQ (TCN) (see Figure 1c), each featuring only one type of the two EWGs of DDQ. For comparison, pentacene (PNT) is also considered (see Figure 1d).

2. Computational Methods and Models

2.1. Quantum Chemical Calculations. Quantum chemical calculations, required to obtain equilibrium structures of the neutral species and molecular ions, were carried out at the B3LYP/6-31G** level of theory (which corresponds to B3LYP/6-31G* for BQ derivatives, because of the lack of light atoms). To estimate the ionization potential of pentacene, Koopmans' theorem[23] was employed, while the vertical electron affinities (VEA) of DDQ and other BQ derivatives were directly estimated as energy differences between neutral and charged species both computed at the geometries optimized for the neutral (VEAn) or the charged (VEAc) species (see also Figure S1). The nature of the critical points determined by quantum-chemical structure optimizations was assessed by evaluating vibrational frequencies at the optimized geometries. Vibrational frequencies were also employed to estimate the vibrational contributions to the intramolecular reorganization energies[24,25] (see below).

The charge transfer integrals V'_{ij} were computed with the INDO[26] or CNDO[27] Hamiltonians following the direct approach described in refs 28−30. The computed transfer integrals V'_{ij} were transformed in an orthogonalized basis (V_{ij}) as described in previous studies.[31] All of the quantum-chemical calculations were carried out with the Gaussian 03 suite of programs.[32]

2.2. Modeling Charge Transport Parameters and Processes. Bulk charge transport was assumed to be governed by the hopping mechanism.[24,25] In this scheme, the relevant charge transfer event is localized on a molecular pair (dimer) formed by two neighboring molecules. The organic semiconductor material was assumed to be in its crystalline form, and the possible dimers were identified by building, for each organic system, a supercell from the unit cell of the crystal structures[33−36] and by evaluating the distances between the centers of mass of the molecules in the supercell. The dimers with distances lower than ca. 10 Å were considered. The different dimers selected for PNT and DDQ are collected in Figures 2 and 3, while those selected for TCQ and TCN are shown in Figures S2 and S3.

There are two parameters governing the hopping process: the charge transfer integral or interaction integral V_{ij} between the two

(15) Caironi, M.; Natali, D.; Canesi, E.; Bianco, A.; Bertarelli, C.; Zerbi, G.; Sampietro, M. *Thin Solid Films* **2008**, *516*, 7680–7684.
(16) Caironi, M.; Natali, D.; Sampietro, M.; Bertarelli, C.; Bianco, A.; Dundulachi, A.; Canesi, E.; Zerbi, G. *Appl. Phys. Lett.* **2006**, *89*, 243519.
(17) Fazzi, D.; Castiglioni, C.; Negri, F.; Bertarelli, C.; Famulari, A.; Meille, S. V.; Zerbi, G. *J. Phys. Chem. C* **2008**, *112*, 18628–18637.
(18) Mukherjee, B.; Batabyal, S. K.; Pal, A. J. *Adv. Mater.* **2007**, *19*, 717–722.
(19) Bandyopadhyay, A.; Chowdhury, A.; Pal, A. J. *Opt. Mater.* **2006**, *28*, 1432–1436.
(20) Mukherjee, B.; Pal, A. J. *Synth. Met.* **2005**, *155*, 336–339.
(21) Mukherjee, B.; Pal, A. J. *Appl. Phys. Lett.* **2004**, *85*, 2116–2118.
(22) Novembre, C.; Guerin, D.; Lmimouni, K.; Gamrat, C.; Vuillaume, D. *Appl. Phys. Lett.* **2008**, *92*, 103314.
(23) Koopmans, T. *Physica* **1934**, *1*, 104–113.
(24) Bredas, J. L.; Beljonne, D.; Coropceanu, V.; Cornil, J. *Chem. Rev.* **2004**, *104*, 4971–5003.
(25) Coropceanu, V.; Cornil, J.; da Silva, D. A.; Olivier, Y.; Silbey, R.; Bredas, J. L. *Chem. Rev.* **2007**, *107*, 926–952.
(26) Pople, J. A.; Beveridge, D.; Dobosh, P. *J. Chem. Phys.* **1967**, *47*, 2026–2033.
(27) Segal, G.; Pople, J. A. *J. Chem. Phys.* **1966**, *44*, 3289–3296.
(28) Orlandi, G.; Troisi, A.; Zerbetto, F. *J. Am. Chem. Soc.* **1999**, *121*, 5392–5395.
(29) Troisi, A.; Orlandi, G. *Chem. Phys. Lett.* **2001**, *344*, 509–518.
(30) Fujita, T.; Nakai, H.; Nakatsuji, H. *J. Chem. Phys.* **1996**, *104*, 2410–2417.
(31) Farazdel, A.; Dupuis, M.; Clementi, E.; Aviram, A. *J. Am. Chem. Soc.* **1990**, *112*, 4206–4214.
(32) Frisch, M. J.; *Gaussian 03*, revision C.02; Gaussian, Inc.: Wallingford, CT, 2004.
(33) Mattheus, C. C.; Dros, A. B.; Baas, J.; Meetsma, A.; de Boer, J. L.; Palstra, T. T. M. *Acta Crystallogr., Sect. C* **2001**, *57*, 939–941.
(34) Zanotti, G.; Bardi, R.; Del Pra, A. *Acta Crystallogr., Sect. B* **1980**, *36*, 168–171.
(35) Vazquez, C.; Calabrese, J. C.; Dixon, D. A.; Miller, J. S. *J. Org. Chem.* **1993**, *58*, 65–81.
(36) Ueda, I. *J. Phys. Soc. Jpn.* **1961**, *16*, 1185–1194.

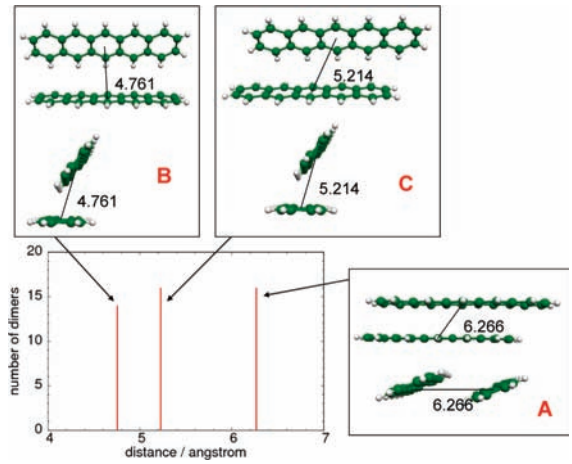

Figure 2. Molecular dimers of PNT extracted from the crystal supercell ($3 \times 2 \times 2$) and considered in the simulation of hopping events. Distances from centers of mass are in angstroms.

molecules i and j forming the dimer and the reorganization parameter λ. The latter is composed by an intramolecular contribution λ_i and an outer contribution λ_o arising from the embedding of the molecular dimer in the crystal.

$$\lambda = \lambda_i + \lambda_o \tag{1}$$

The intramolecular reorganization parameters were computed with the B3LYP functional, either with the adiabatic potential (AP) approach[24,37] (see Figure S1 in the Supporting Information and Table 1) or via calculations of Huang−Rhys (HR) parameters.[24,37]

The HR parameters S_m can be obtained from the dimensionless displacement parameters B_m usually employed in the evaluation of the Franck−Condon (FC) vibronic progressions in electronic spectra.[38,39]

The latter, assuming the harmonic approximation, are defined as

$$B_m = \sqrt{\frac{\omega_m}{\hbar}}\{\mathbf{X}_K - \mathbf{X}_J\}\mathbf{M}^{1/2}\mathbf{L}_m(K)$$
$$S_m = \frac{1}{2}B_m^2 \tag{2}$$

where $\mathbf{X}_{K,J}$ is the $3N$ dimensional vector of the equilibrium Cartesian coordinates of the K,Jth state (here the neutral and charged molecular states), $\mathbf{M}$ is the $3N \times 3N$ diagonal matrix of the atomic masses, and $\mathbf{L}_m(K)$ is the $3N$ vector describing the normal coordinate Q_m of the K state in terms of mass-weighted Cartesian coordinates.

Each hopping event was considered as a nonadiabatic charge transfer reaction, and the transfer rate constants k_{eT} were computed according to the Marcus−Levich−Jortner (MLJ) formulation:[40,41]

$$k_{eT} = \frac{2\pi}{\hbar}V_{ij}^2\frac{1}{\sqrt{4\pi\lambda_o k_B T}}\sum_{v=0}^{\infty}\left[\exp(-S_{eff})\frac{S_{eff}^v}{v!}\times \exp\left(-\frac{(\Delta G^\circ + \lambda_o + v\hbar\omega_{eff})^2}{4\lambda_o k_B T}\right)\right] \tag{3}$$

In the expression above, V_{ij} are the charge transfer integrals, λ_o is the outer reorganization parameter, and ΔG° is zero for the self-exchange processes considered in this work ($M^0 + M^c \leftrightarrow M^c + M^0$, M^0 being the organic species in the neutral state, M^c being the organic species in its charged state). Equation 3 includes the quantum description of the nonclassical degrees of freedom represented by a single effective mode of frequency ω_{eff} and associated HR factor S_{eff}. The effective frequency was determined as

$$\omega_{eff} = \sum_m \omega_m \frac{S_m}{\sum_n S_n} \tag{4}$$

and the HR factor S_{eff} follows from the relation $\lambda_i = \hbar\omega_{eff} \cdot S_{eff}$.

The outer-sphere reorganization energy λ_o cannot be easily estimated for charge transport processes in solid state media. Here, we have taken λ_o as a parameter equal to 0.1 eV, in keeping with recent studies.[42,43] We are conscious that the absolute values of the rate constants can be strongly influenced by the chosen outer-sphere reorganization energy parameter. In addition, the validity of the nonadiabatic hopping model depends on the relative magnitude of the charge transfer integral V_{ij} and the reorganization parameter λ, with V_{ij} required to be considerably smaller than λ.[25,44] As it will be shown, we are within this limit only for the BQ derivatives, and for this reason the results on pentacene connected with the hopping assumption will not be presented in the following discussion. The temperature range is also relevant, because the hopping contribution dominates in the high temperature regime, which is the one considered in this work.

Charge mobilities were computed assuming a Brownian motion of the charge carrier.[45] The calculation of the macroscopic parameter was performed by considering the three-dimensional crystal structures of PNT,[33] DDQ,[34] TCQ,[36] and TCN[35] and by computing the diffusion coefficient D with the approximate relation[45] providing a qualitative estimate of D:

$$D = \frac{1}{2d}\sum_n (r_n)^2 k_n P_n \tag{5}$$

Here, n runs over possible hopping events for a charge localized on a given molecular unit in the crystal, d is the dimensionality of the system, r_n is the distance between the starting molecule and the neighboring molecule in the hopping event, and finally P_n is the probability associated with the hopping, determined by the charge transfer rate constant k_n.

$$P_n = \frac{k_n}{\sum_j k_j} \tag{6}$$

Charge mobility is readily obtained as

$$\mu = \frac{eD}{k_B T} \tag{7}$$

To assess the importance of thermal motions in the modulation of the charge transfer integrals relevant for the charge transport, we run molecular dynamics simulations on a supercell ($2 \times 2 \times 4$) of the crystal unit cell of DDQ.[34] The dynamics of the system was studied with periodic boundary conditions employing the MM3 force field[46] and the Tinker code.[47] It has been shown in recent studies that low frequency intermolecular vibrations can modulate the magnitude of the charge transfer integrals.[48] Thus, we froze all

(37) Coropceanu, V.; Andre, J. M.; Malagoli, M.; Bredas, J. L. *Theor. Chem. Acc.* **2003**, *110*, 59–69.
(38) Negri, F.; Orlandi, G. *J. Chem. Phys.* **1995**, *103*, 2412–2419.
(39) Negri, F.; Zgierski, M. Z. *J. Chem. Phys.* **1995**, *102*, 5165–5173.
(40) Marcus, R. A. *J. Chem. Phys.* **1956**, *24*, 966–978.
(41) Jortner, J. *J. Chem. Phys.* **1976**, *64*, 4860–4867.
(42) Koh, S. E.; Risko, C.; da Silva, D. A.; Kwon, O.; Facchetti, A.; Bredas, J. L.; Marks, T. J.; Ratner, M. A. *Adv. Funct. Mater.* **2008**, *18*, 332–340.
(43) Norton, J. E.; Bredas, J. L. *J. Am. Chem. Soc.* **2008**, *130*, 12377–12384.
(44) Cheung, D. L.; Troisi, A. *Phys. Chem. Chem. Phys.* **2008**, *10*, 5941–5952.
(45) Song, Y.; Di, C.; Yang, X.; Li, S.; Xu, W.; Liu, W.; Yang, L.; Shuai, Z.; Zhang, D.; Zhu, D. *J. Am. Chem. Soc.* **2006**, *128*, 15940–15941.

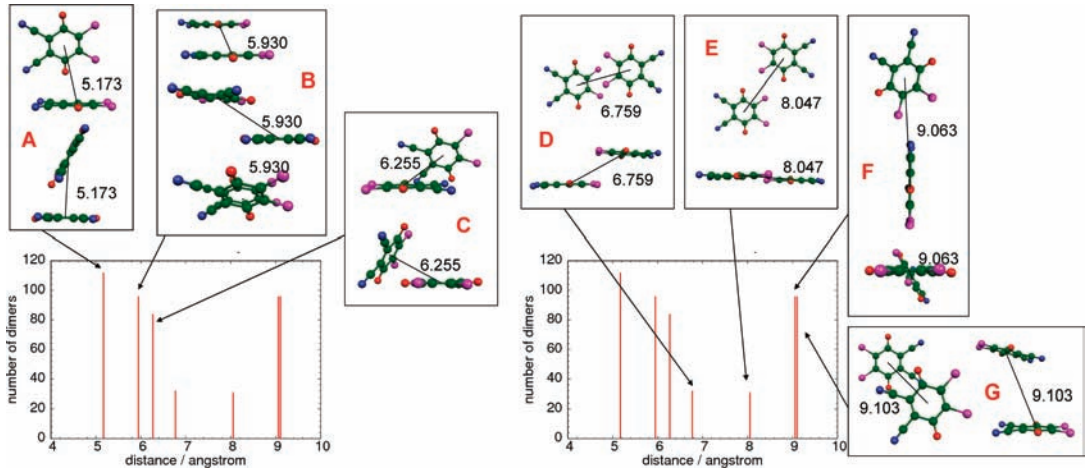

Figure 3. Molecular dimers of DDQ extracted from the crystal supercell (2 × 2 × 4) and considered in the simulation of hopping events. Distances from centers of mass are in angstroms.

Table 1. Intramolecular Reorganization Energies (eV) Computed for DDQ, TCQ, TCN (B3LYP/6-31G*), and PNT (B3LYP/6-31G**)

	$\lambda_i^{n(AP)a}$	$\lambda_i^{c(AP)b}$	$\lambda_i^{n(HR)c}$	$\lambda_i^{c(HR)d}$	λ_i^{AP}	λ_i^{HR}
PNT	0.05	0.05	0.05	0.05	0.10	0.10
DDQ	0.21	0.21	0.21	0.21	0.42	0.42
TCQ	0.26	0.26	0.26	0.26	0.52	0.52
TCN	0.17	0.16	0.17	0.17	0.33	0.34

[a] Contribution from the neutral system, computed according to the AP method. [b] Contribution from the charged system, computed according to the AP method. [c] Contribution from the neutral system, computed from the HR parameters. [d] Contribution from the charged system, computed from the HR parameters. See also Figure S1 in the Supporting Information for a graphical representation of the reorganization energies.

of the intramolecular degrees of freedom and kept the molecule in the cell rigid at its crystal structure while allowing intermolecular motions. We run MD simulations in the NVT ensemble at T = 100 and 300 K, using the Berendsen's algorithm[49] to simulate the presence of a thermal bath. The integration time step was set to 1 fs. The transfer integrals between LUMO orbitals were evaluated every 60 fs for the different dimers identified in the crystal of DDQ (see Figure 3). Fourier transforms of the autocorrelation function of the transfer integrals were also evaluated to extract the phonon frequencies, leading to more effective coupling modulation.[48,50,51]

3. Results and Discussion

The molecular memory device configuration is made by a layer of the organic molecular semiconductor material sandwiched between two electrodes, usually ITO and Al.[4] Experiments on DDQ indicate that the redox process occurring at the electrode/organic semiconductor interface is a reduction,[19] due to its electron-withdrawing properties in turn connected with its n-type semiconductor character. We assumed a reduction process for the other BQ derivatives, also characterized by the presence of the same EWGs of DDQ, while the relevant redox process was assumed to be an oxidation for PNT, due to its p-type semiconductor character. The bistability of the memory device can be discussed by considering the two major processes that can contribute to the current−voltage characteristic shape. These are (1) the charge injection at the electrode−semiconductor interface and (2) the charge transport across the organic material. In the following, we discuss the efficiencies of both processes on the basis of computed intramolecular and intermolecular parameters.

3.1. Electrode/Organic Interface Charge Transport and Molecular Electronic Levels. To discuss the injection across the electrode/organic material interface, we assume the validity of the Schottky rule[53] and compare the work function of the electrode with the relevant transport levels of the organic materials. Experimentally, those levels are obtained from photoelectron or inverse photoelectron spectra, and the electronic affinity (EA) and ionization potential (IP) of the solid material are conventionally associated with the one-electron levels measured from photoelectron experiments.[54,55]

Accordingly, we computed the VEAn of BQ derivatives in the gas phase with B3LYP/6-31G* calculations on neutral and charged species and compared them to the work function of common electrodes. The energy offset between the electrode/organic material levels determines the injection barrier. Experimental EAs of the solid phases of BQ derivatives are not known. However, it is known that when a molecule is part of a condensed phase of identical molecules, additional forces of interaction come into play, markedly altering the energetic of ionization and electron attachment. A major factor in this alteration is the stabilizing effect of the polarization. The polarization energy of stabilization in the organic crystal is qualitatively comparable to the solvation energy of ions in solution,[52] and it has been recently investigated by QM/MM calculations.[43] Accordingly, we corrected the computed gas-phase values by assuming polarization effects of the order of 0.5 eV. A schematic representation of the electronic levels at the electrode/semiconductor interface is shown in Figure 4a for

(46) Allinger, N. L.; Yuh, H. Y.; Lii, J. H. *J. Am. Chem. Soc.* **1989**, *111*, 8551–8566.
(47) Ponder, J. W. *TINKER, Software Tools for Molecular Design version 4.2*; 2004.
(48) Troisi, A.; Orlandi, G. *J. Phys. Chem. A* **2006**, *110*, 4065–4070.
(49) Berendsen, H. J. C.; Postma, J. P. M.; van Gusteren, W. F.; Di Nola, A.; Haak, J. R. *J. Chem. Phys.* **1984**, *81*, 3684–3690.
(50) Troisi, A.; Orlandi, G.; Anthony, J. E. *Chem. Mater.* **2005**, *17*, 5024–5031.
(51) Troisi, A. *Adv. Mater.* **2007**, *19*, 2000–2004.
(52) Pope, M.; Swenberg, C. E. *Electronic Processes in Organic Crystals and Polymers*; Oxford University Press: New York, Oxford, 1999; p 1328.
(53) Schottky, W. *Z. Phys.* **1942**, *118*, 539–592.
(54) Kahn, A.; Koch, N.; Gao, W. *J. Polym. Sci., Part B: Polym. Phys.* **2003**, *41*, 2529–2548.
(55) Gao, W.; Kahn, A. *Org. Electron.* **2002**, *3*, 53–63.

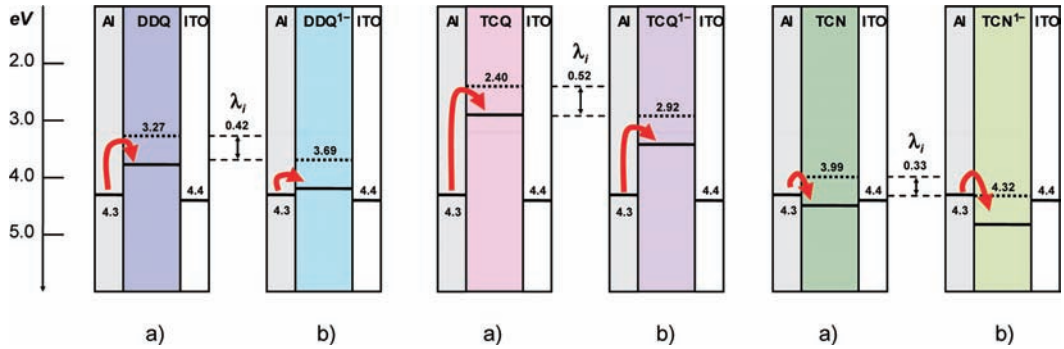

Figure 4. B3LYP/6-31G* computed (eV, dashed lines) VEAs at the equilibrium structures of (a) neutral (VEAn) and (b) negatively charged (VEAc) species along with their difference corresponding to λ_i. DDQ (left), TCQ (center), and TCN (right). Comparison with the work function of ITO and Al electrodes (eV).[16] Solid lines below dashed lines represent schematically the stabilizing effect of polarization energy in the organic crystal.[52] Red arrows show the electron injection process from the electrode.

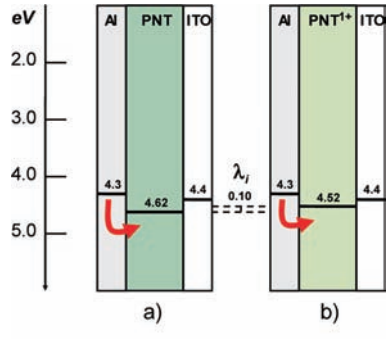

Figure 5. B3LYP/6-31G** HOMO energies (eV) of PNT at the equilibrium structure of (a) neutral and (b) positively charged species along with their difference corresponding to λ_i. Comparison with the work function of ITO and Al electrodes (eV).[16] Red arrows show schematically the hole injection process from the electrode.

the BQ derivatives and in Figure 5a for PNT. Besides the computed gas-phase values of the VEAn (dashed lines), comparing well with the results of previous calculations[56] and with the experimental data,[57] in Figure 4a we also indicate with solid lines the more realistic levels including the effect of polarization. For PNT, the IP was estimated directly from the B3LYP/6-31G** HOMO energy because this is predicted, for a favorable error cancelation, quite close to the experimental IP of ca. 5.0 eV in the condensed phase.[52] From the computed levels, it is apparent that electron injection either from Al or from ITO will be an activated process for all of the systems studied except for TCN whose VEAn level suggests a barrierless injection. In the figure, the red arrows indicate the electron injection assumed to occur from the Al electrode. The increased level alignment moving from TCQ to TCN is a result of the increased strength of EWGs.

As the voltage creates the reduced state, modified energy levels of the molecules have to be considered to discuss the charge injection at the interface. In some cases, these modified levels become better aligned with the electrode work functions. To estimate the modified alignment, we determined the VEAc at the equilibrium structures of the charged species. The computed equilibrium structures of the four molecules in their neutral and charged configurations are collected in the Supporting Information (Figures S4−S7). For BQ derivatives, the major geometry change upon electron doping is the transition from a quinoid to a more benzenoid structure. For PNT, the geometry change induces elongation of the CC bonds mainly along the short molecular axis. The structural changes associated with negative charging of DDQ and other BQ derivatives are reflected in an increase of the VEAc as compared to the VEAn (see Figure S1 in the Supporting Information). A graphical representation of the relevant electronic levels associated with charging is given in Figure 4b for BQ derivatives and in Figure 5b for PNT. It is seen that VEAc increases in all cases, as compared to the VEAn, the increase being inversely related with the strength of the EWGs. Accordingly, TCQ shows the larger increase and TCN shows the smaller. It should be noted that the VEA change (the reduction of the injection barrier for electrons) is equivalent to the reorganization energy λ_i associated with the charging process (see also Figure S1 in the Supporting Information). The computed EA changes suggest an improved level alignment at the heterojunction in the case of DDQ and TCQ. In contrast, for TCN, the computed VEAs suggest that alignment with the work function of the Al electrode should be already very efficient for the pristine BQ derivative. Thus, while for DDQ a remarkably increased charge injection at the electrode/organic interface is expected, such effect is not expected to be significant for TCN. Finally, in the case of TCQ, one expects the switch to occur at higher applied voltages. Furthermore, the sizable VEAc increase upon charging (large λ_i) that would play a positive role in determining the efficiency of the memory device is likely to be insufficient to sustain efficient charge injection (at low applied voltages), due to the large computed injection barrier. Estimates taking into account interfacial dipoles formation will be required to confirm this conjecture.[58,59] In summary, the appropriate VEAn level alignment with the work function of the electrode, combined with a considerable VEAc increase (a sizable λ_i), seems to be better realized with DDQ, the only BQ derivative that has been shown to display the resistive memory effect.[4,8] The observed electrode-dependent ON (and OFF) state currents displayed by DDQ[4] can be easily accounted for by the present interpretative scheme. According to the calculations, when charged molecules are created at the interface (for an applied voltage V above a threshold value), a sudden increase of current is expected as a

(56) Boesch, S. E.; Grafton, A. K.; Wheeler, R. A. *J. Phys. Chem.* **1996**, *100*, 10083–10087.
(57) Chen, E. C. M.; Wentworth, W. E. *J. Chem. Phys.* **1975**, *63*, 3183–3191.
(58) Ishii, H.; Sugiyama, K.; Ito, E.; Seki, K. *Adv. Mater.* **1999**, *11*, 605–625.
(59) Vazquez, H.; Flores, F.; Oszwaldowski, R.; Ortega, J.; Perez, R.; Kahn, A. *Appl. Surf. Sci.* **2004**, *234*, 107–112.

result of the concomitant barrier reduction at the interface, following the change from VEAn to VEAc.

From a mechanistic point of view, the charged species at the interface will transfer its electron to a nearby neutral molecule, farther away from the interface, through a hopping event that drives the electron current transport across the organic material. At the same time, before intramolecular relaxation occurs in the neutralized molecule at the interface, ultrafast electron transfer from the electrode is facilitated by the increased electron affinity of the molecule. Such ultrafast event would be facilitated by the formation of an electrode−organic molecule complex.[58,59]

Applying the same considerations as above to PNT, we can conclude that due to the minor HOMO level rearrangement occurring upon oxidation (see Figure 5), a negligible change in hole injection at the electrode is expected. This conclusion, based on the intramolecular properties of PNT, is in agreement with the observed negligible memory effect displayed by PNT in the absence of other extrinsic mechanisms such as the inclusion of metal nanoparticles.[5] To summarize, the examples considered above underscore the possible relevant role of the intramolecular reorganization parameter λ_i of the organic material in governing the efficiency of the resistive memory device. It should be noted that this conclusion agrees with the better memory performance of the Z form of DPBT derivatives.[17] A schematic macroscopic representation of the memory phenomenon taking into account the role of the intramolecular parameters is shown in Figure 6.

3.2. Intra- and Intermolecular Parameters for Bulk Charge Transport. Besides the process at the electrode/organic interface, controlled by intramolecular parameters possibly governing the efficiency of the transition from the OFF to the ON state of the memory device, one has to consider also the charge transport across the organic material, whose efficiency will contribute to sustain charge density in the organic material, and hence the ON state. In this context, it should be noted that the sizable λ_i required for an efficient ON/OFF ratio plays against the efficiency of the charge transport as indicated by the MLJ rate constant formulation (eq 3). To further clarify this point, we modeled the charge transport process assuming a nonadiabatic hopping mechanism and computed the required parameters entering the MLJ eq 3. The intramolecular reorganization energies λ_i are collected in Table 1, while the effective parameters employed in the calculation of rate constants are summarized in Table 2. The λ_i were evaluated with the AP method and by computing the HR parameters determining the vibrational FC factors. A detailed analysis of the vibrational contributions to the reorganization energies is provided in the Supporting Information, Tables S1 and S2, Figures S8−S15. As discussed in the previous section, BQ derivatives show considerably larger λ_i as compared to PNT. These, on the other hand, agree with previous literature data[37,60] for PNT. Because of the different FC contributions of PNT and BQ derivatives, the ω_{eff} entering eq 3 is considerably different: 1317 cm^{-1} for PNT, 780 cm^{-1} (DDQ), 811 cm^{-1} (TCQ),and 681 cm^{-1} (TCN) for BQ derivatives (see Table 2). The charge transport integrals V_{ij}, required to estimate the rate constants, are collected in Table 3, while the corresponding LUMO and HOMO orbitals are collected in Figure S16. The computed rate constants of BQ derivatives (a selection of the largest is collected in Table 4) were employed to estimate charge mobilities according to eqs 5−7 and assuming a crystalline state for the layer of the organic material in the device. The temperature dependence of the computed mobilities is shown in Figure S17. It is seen that the three BQ derivatives show considerably smaller mobilities as compared to PNT, whose computed value at 300 K, using the same approach, is ca. 1.3 $cm^2\ V^{-1}\ s^{-1}$. The reduced mobilities can be attributed to the reduced electronic factors (the largest

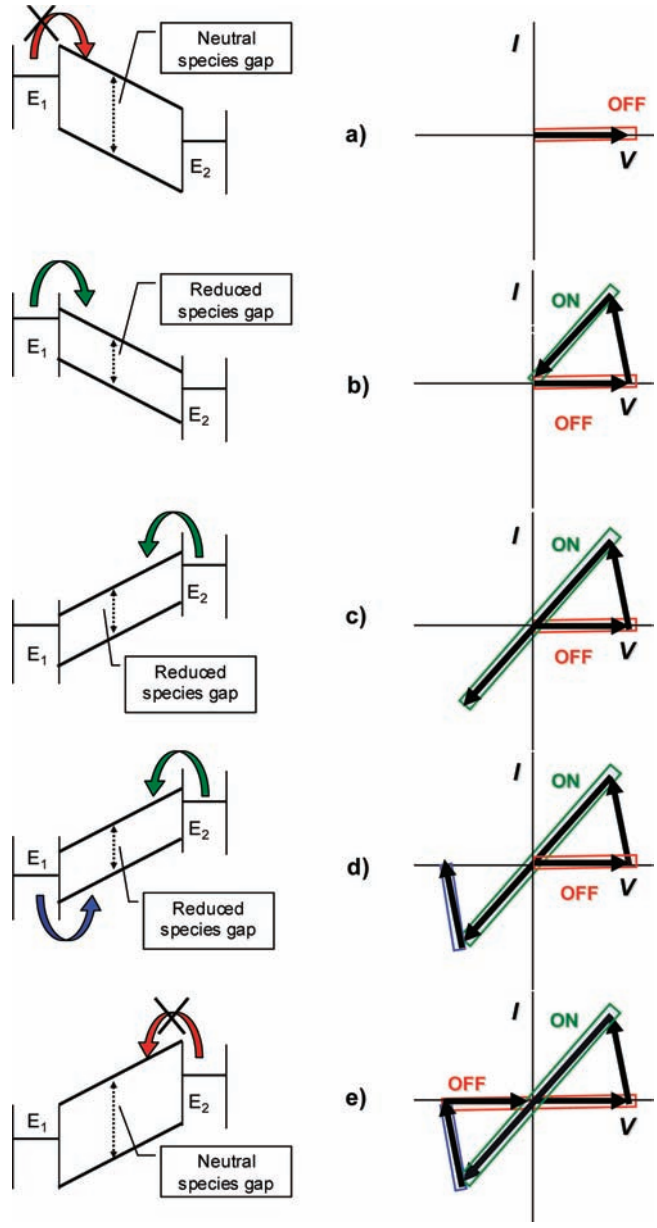

Figure 6. Schematic macroscopic representation of the electric bistability of a memory device based on an n-type molecular semiconductor wafered between electrodes E_1 and E_2. Device levels (left); schematic current−voltage ($I-V$) curve as a function of the voltage scan (right). The most relevant processes at the interface are indicated. (a) Initially the device is in its OFF state, and the transport gap is that of the pristine semiconductor. (b) As the applied voltage reaches the threshold value, the improved work function/VEA alignment favors electron injection. When charged species are at the interface, energy levels associated with the charged species have to be considered, further improving the electron injection. The system switches to the ON state. (c) As long as charge carriers are sustained in the device, the system stays in the ON state also for reverse applied voltages. (d) When the second (reverse) threshold voltage is reached, hole injection becomes competitive and neutralization of the charged species becomes significant, leading to a switch of the system back to the OFF state. (e) The transport gap reverts to that of the neutral species, and the system retains the OFF state.

(60) Malagoli, M.; Coropceanu, V.; da Silva, D. A.; Bredas, J. L. *J. Chem. Phys.* **2004**, *120*, 7490–7496.

Table 2. Effective Frequency ω_{eff} and Associated HR Factor S_{eff} Employed in the Evaluation of Charge Transfer Rate Constants of DDQ, TCQ, TCN (B3LYP/6-31G*), and PNT (B3LYP/6-31G**)

	PNT	DDQ	TCQ	TCN
ω_{eff} (cm^{-1})	1317	780	811	681
S_{eff}	0.57	4.42	5.22	3.98

Table 3. Charge Transfer Integrals V_{ij} (cm^{-1}) of DDQ, TCQ, TCN, and PNT, Computed for the Most Relevant Dimers Extracted from the Crystal Structures

	DDQ		TCQ		TCN	
dimer	distance (Å)	$^{a}V_{ij}^{LUMO}$	distance (Å)	$^{a}V_{ij}^{LUMO}$	distance (Å)	$^{a}V_{ij}^{LUMO}$
A	5.173	−436	5.303	−494	6.213	−190
B	5.930	387	5.830	417	6.668	23
C	6.255	−161	8.760	35	6.989	35
D	6.759	24	8.860	0	7.142	171
E	8.047	−40	9.036	−48	7.483	−29
F	9.063	−24			7.657	40
G	9.103	0				

	PNT	
dimers	distance (Å)	$^{b}V_{ij}^{HOMO}$
A	4.761	−807
B	5.214	557
C	6.266	395

[a] Charge transfer integrals were evaluated at CNDO level.[27] The interaction was determined between the LUMO orbitals of the two molecules belonging to the dimer. [b] Charge transfer integrals evaluated at INDO level.[26] The interaction was determined between the HOMO orbitals of the two molecules belonging to the dimer.

Table 4. Selection of the Largest Computed MLJ Charge Transfer Rate Constants k_{eT} (at 300 K) of DDQ, TCQ, and TCN[a]

	DDQ		TCQ		TCN	
dimer	distance (Å)	k_{eT} (s^{-1})	distance (Å)	k_{eT} (s^{-1})	distance (Å)	k_{eT} (s^{-1})
A	5.173	9×10^{11}	5.303	5.6×10^{11}	6.213	2.8×10^{11}
B	5.930	6.8×10^{11}	5.830	4.0×10^{11}		
C	6.255	1.2×10^{11}				
D					7.142	2.3×10^{11}

[a] The dimers to which computed rates correspond are also indicated.

charge transfer integral of BQ derivatives is about one-half of the largest transfer integral of PNT) and the concomitant increase of the intramolecular reorganization energies whose effect is to depress the efficiency of the charge transfer event. The mobilities were computed assuming the values of the V_{ij} computed at the crystal geometry. However, it has been shown that the effect of thermally induced disorder on the V_{ij} can be substantial.[48,51] Accordingly, we run molecular dynamics simulations at 100 and 300 K and evaluated the charge transfer integrals for a series of sampled configurations. The thermally induced dynamic effects can be appreciated by inspecting Figure 7a showing broad Gaussian distributions of the computed V_{ij} values (see also Figure S18 in the Supporting Information), as it was shown in previous studies on oligoacenes.[48,50,51] It is seen that V_{ij} values are subject to oscillations of the same magnitude of the integrals and that the width of the Gaussian distribution increases with temperature. It can be concluded that the thermal disorder effects on V_{ij} are a very general property encompassing high mobility and less efficient organic semiconductors. More detailed information on the frequencies of the intermolecular modes modulating the charge transport integrals can be extracted from the

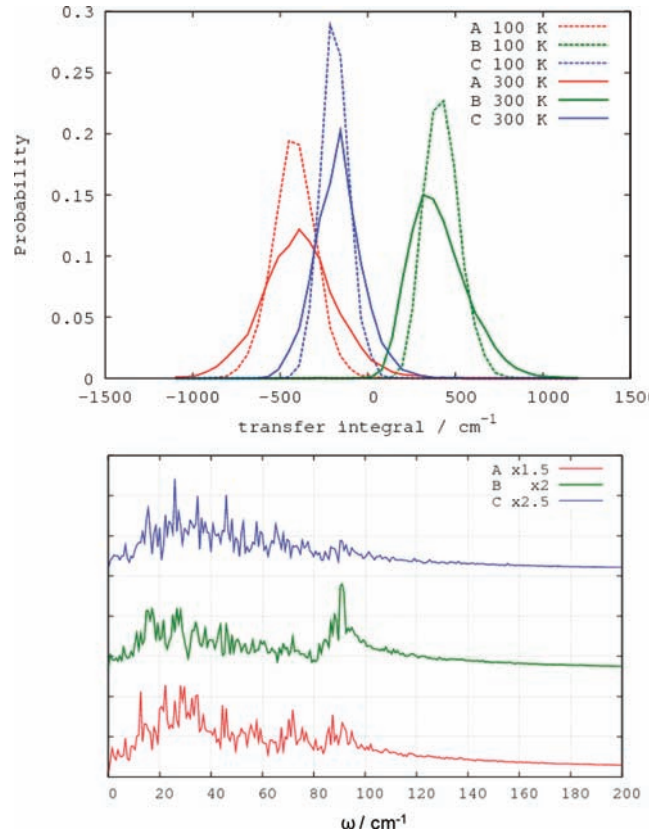

Figure 7. Thermal disorder effects on the distribution of the largest computed charge transfer integrals of DDQ (top) evaluated at two temperatures (100 and 300 K) and Fourier transforms of the autocorrelation function of the transfer integrals computed at 300 K (bottom) underscoring the low frequency active modes responsible for the modulation of the charge transfer integrals.

Fourier transforms of the autocorrelation functions of the V_{ij} shown in Figure 7b. Similarly to previous studies on the more efficient oligoacene semiconductors,[48,50,51] we find that low frequency intermolecular modes in the range 20−80 cm^{-1} modulate the integrals. Interestingly, computed rate constants (see Table 4) are of the order of $1 \div 10 \times 10^{11}$ s^{-1}, indicating that nuclear motions, associated with frequencies in the range of few tens of cm^{-1} as those modulating the V_{ij}, can effectively contribute to alter the charge transfer rate constants and the computed mobilities. It is clear, however, that the effect of the sizable intramolecular reorganization parameters computed for BQ derivatives is to depress the mobilities as compared to those of highly conductive oligoacenes. Thus, we can conclude that the balance between efficient ON/OFF ratio and efficient transport in the bulk is strongly influenced by the intrinsic molecular properties of the organic material. In the case of PNT, the small λ_i value favors the efficient charge transport but disfavors the ON/OFF ratio in memory devices. In contrast, for DDQ the appropriate combination seems to be realized, and it results in a favorable ON/OFF ratio without compromising the charge transport across the organic material. The reorganization energy parameters are sizable also for TCQ and TCN, but in these cases inefficient level alignment (TCQ) or too efficient injection in the pristine material (TCN) is expected to result in less efficient memory effects. It can be speculated that, for a memory device, if the λ_i becomes even larger, the gain in the ON/OFF ratio will be negatively compensated by the hampered charge transport of the highly trapped charge carriers across the organic material.

4. Concluding Remarks

We have investigated, by means of computed intra- and intermolecular parameters, the intrinsic molecular nature of the memory effect displayed by DDQ, TCQ, and TCN, a series of BQ derivatives exhibiting EWGs of different strength, and PNT, an example of a highly conducting oligoacene. Two relevant processes have been considered: the efficiency of the charge injection at the electrode/organic interface and the charge transport across the organic material.

Concerning the first process, calculations suggest that the OFF state is injection limited, determined by the activated process of charge injection in most of the systems investigated. The strength and the number of EWGs improve level alignment of the pristine material and reduce the barrier to electron injection. With regard to the switching from the OFF (low conductivity) to the ON (high conductivity) state, the systems investigated underscore the relevant role of the intramolecular reorganization energy λ_i in governing the efficiency of the resistive memory device, in particular the ON/OFF ratio, through the modulation of the level alignment in the presence of charged species at the interface. Indeed, when charged species are at the interface, energy levels associated with the charged species have to be considered, further improving the electron injection. The increased alignment has been shown to be related to a sizable reorganization energy λ_i.

Employing the MLJ formalism to estimate the efficiency of the charge hopping mechanism, it has been shown that the sizable λ_i providing an efficient ON/OFF ratio, combined with moderate charge transfer integrals, depresses the bulk charge transport of DDQ and other BQ derivatives as compared to the highly conductive PNT. To extend our understanding of the charge transport mechanism in these semiconductors, we have evaluated the effect of thermally induced disorder on computed charge transfer integrals. Similarly to previous studies on oligoacene semiconductors, we have found that low frequency intermolecular modes in the range $20-80$ cm^{-1} modulate the integrals.

The role of molecular parameters disclosed by this study might be exploited for tuning the bistability behavior of new molecular-based semiconductors and to gain control of the memory phenomenon by appropriate design rules. Studies on other molecular semiconductors displaying electrical bistability are in progress.

Acknowledgment. This work was supported by funds from MIUR: grant ex 60%, PRIN Project 2007 NZLYE5_001 "Energy and charge transfer: from collisions to dissipative processes", and FIRB project RBNE033KMA "Molecular compounds and hybrid nanostructure materials with resonant and non-resonant optical properties for photonic devices". We are indebted to Prof. Magda Monari for assistance with the access to the Cambridge Crystallographic Data Centre.

Supporting Information Available: Three tables including computed HR parameters and computed absolute energies. Eighteen figures including a scheme for the calculations of VEAs and λ_i, a representation of the dimers extracted from the crystal of TCQ and TCN, the geometries of neutral and charged species, the detailed analysis of the computed vibrational contributions to the λ_i, the molecular orbitals involved in the charge transfer process, the computed temperature-dependent mobilities, and the fluctuations of computed charge transfer integrals for DDQ. In addition, the Cartesian coordinates of all of the optimized structures and complete ref 32. This material is available free of charge via the Internet at http://pubs.acs.org.

JA901101C